Article

Evaluation of the Applicability of the ERA5 Reanalysis for Interpretation of the Polarization Laser Sensing Data of the High-Level Clouds in Western Siberia

Ilya Bryukhanov [1,], Maxim Penzin [2], Olesia Kuchinskaia [2*], Evgeny Ni [1], Konstantin Pustovalov [3,4], Valentina Bryukhanova [1], Nikolay Kirillov [1], Ivan Zhivotenyuk [1], Anton Doroshkevich [1], Alexander Stykon [1], Iurii Bordulev [2,5], Vadim Kostyukhin [2], and Ignaty Samokhvalov [1]

[1] Department of optoelectronic systems and remote sensing, Faculty of Radiophysics, National Research Tomsk State University, 634050 Tomsk, Russia; wolf.ni@yandex.ru (E.N.); leo@mail.tsu.ru (V.B.); knsnik@gmail.com (N.K.); guitarplayer@mail.tsu.ru (I.Zh.); antdoro@mail.ru (A.D.); stikon@yandex.ru (A.S.); lidar@mail.tsu.ru (I.S.)

[2] Laboratory for Analysis of High Energy Physics Data, Faculty of Physics, National Research Tomsk State University, 634050 Tomsk, Russia; penzin.maksim@gmail.com (M.P.); olesyatsu14@mail.ru (O.K.); bordulev@gmail.com (Iu.B.)

[3] Laboratory of Physics of Climatic Systems, Institute of Monitoring of Climatic and Ecological Systems of the Siberian Branch of the Russian Academy of Sciences, 634055 Tomsk, Russia; const.pv@yandex.ru (K.P.)

[4] Department of Meteorology and Climatology, Faculty of Geology and Geography, National Research Tomsk State University, 634050 Tomsk, Russia

[5] Division for Experimental Physics, National Research Tomsk Polytechnic University, 634050 Tomsk, Russia

* Correspondence: olesia.kuchinskaia@cern.ch; Tel.: +7-923-421-77-13

Abstract: This article presents results of the polarization laser studies of the optical and microphysical characteristics of the high-level clouds (HLC). The high-altitude matrix polarization lidar (HAMPL; Tomsk, Russia) is described. HAMPL measures vertical profiles of all elements of the backscattering phase matrix (BSPM) of the HLC. Based on the joint analysis of lidar and radiosonde observations it is shown that the spatial structure of the HLC containing oriented ice crystals is inhomogeneous in the horizontal wind direction. It includes local areas with oriented particles; the sizes of such areas are estimated together with the most probable meteorological conditions of their formation. The shortcomings of the radiosonde observations performed closest to the location of the HAMPL are described. The applicability of the ERA5 reanalysis data of the European Centre for Medium-Range Weather Forecasts for use as an alternative source of information on the vertical profiles of meteorological quantities for the interpretation of HLC lidar sensing data in Western Siberia was checked.

Keywords: atmosphere; high-level clouds; ice particles; polarization lidar; interpretation of lidar data; radiosonde observations; ERA5 reanalysis.

1. Introduction

More and more noticeable climatic changes on the Earth determine the need to improve weather and climate forecasts. Increasing the accuracy of atmospheric forecasting requires increasing the completeness, spatio-temporal resolution and accuracy of meteorological information, as well as an in-depth understanding of phenomena occurring in the atmosphere, its structure, composition and dynamics. Cloudiness is not only a regulator of the radiation balance in the Earth's climatic system, but also the most important factor determining the inflow of solar energy to its surface [1–3]. Optical and microphysical models of the atmosphere remain imperfect.

Influence of the high-level clouds (HLC) on the radiative balance in climatic atmospheric models is still not understood[4,5]. Having a large horizontal size reaching thousands of kilometres, such clouds can cover up to half of the Earth's surface [6,7]. The HLC

contribution to the greenhouse effect is significant despite their small optical thickness [8–10]. Special features of HLC optical transmittance are determined by their microstructure, characterised by the distribution of ice particles in the cloud in shape, size, and spatial orientation. These features depend on meteorological conditions in the upper troposphere. The particles can be oriented horizontally, which increases the reflection coefficient and leads to anomalous (specular) backscattering of optical radiation when sensing into the zenith. Existing atmospheric models, including the global atmospheric model by European Centre for Medium-Range Weather Forecasts (ECMWF), do not take into account features of the HLC microstructure. In contrast to droplet clouds, it is difficult to accurately describe sizes and shapes of particles in crystalline or mixed clouds. Usually, the concept of "effective radius" is used, based on equality of one of the properties of particles and a certain model sphere [1]. This simplification allows the use of the Mie theory in calculating radiative characteristics of the HLC, but it is quite coarse and negatively affects the accuracy of numerical weather and climate forecasts.

Experimental studies of HLC are labour-intensive and expensive. There is no instrument for contact determination of the spatial orientation of particles in clouds, because it is violated during air sampling. The theoretical description of optical radiation interaction with nonspherical ice particles is a complex multicomponent task. Modern instruments and methods for experimental data processing bring us closer to the tools that allow adequately relate the characteristics of the HLC with meteorological conditions and predict the microstructure of the clouds being formed. The use of polarization lidar, which provides evaluation of particle orientation along with other parameters (shape and size of ice particles) of the microstructure, makes it possible to compensate for the impossibility to determine the orientation of particles in HLC by contact.

Contrails of planes also have optical properties similar to those of natural HLC. They not only attenuate solar radiation flux themselves, but also form cirrus [11] (e.g., Cirrus floccus homomutatus and Cirrus fibratus homomutatus [12]). The contrails existing more than 10 minutes are named by the World Meteorological Organisation as the only artificial type of ice clouds [13]. Many years of HLC observations in northern latitudes [11] have shown an increase in the frequency of clouds formation with the growth of air traffic. Instrumental studies of the contrail characteristics are difficult, because the contact aircraft-based instruments provide little information (in addition, information on the orientation of ice particles gets lost), and from space platforms traces of aircrafts at the initial stage of formation are not distinguishable from space platforms due to their small dimensions. They become detectable by satellites 1-2 h after the emission of combustion products from aircraft engines, which is too long because the average time of existence of the contrail is about 1-6 h [14].

There are two main problems in developing optical models of crystalline HLC that adequately reflect their microphysical characteristics. The first one is the absence of the certified instrumental methods for determining the orientation of nonspherical particles in the atmosphere at altitudes of the HLC formation. The second one is a complexity of calculations of the basic optical and radiative characteristics of such clouds.

2. Materials and Methods

In the present work, the high-altitude matrix polarization lidar (HAMPL) developed at National Research Tomsk State University is used to measure the vertical profiles of atmospheric parameters. Experiments on HLC sensing have been regularly carried out since 2009 at any time of the day, as long as there is no precipitation, no gusty wind, and low cloud cover. A distinctive feature of the lidar is an ability to perform all measurements necessary for the experimental determination of the vertical profile of the backscattering phase matrix (BSPM) of the HLC layers [15]. Existing analogues (e.g. [16–18]) allow determining only some elements of the BSPM of the HLC, and the rest are calculated based on the symmetry properties of such matrices.

2.1. High-altitude matrix polarization lidar of National Research Tomsk State University

A block diagram of the HAMPL is shown in Figure 1. The lidar is oriented vertically in the zenith direction. A Nd:YAG laser with an operating wavelength of 532 nm, pulse energy up to 400 mJ, and a pulse repetition rate of 10 Hz is used as an optical radiation source. On output of the receiving optical channel of the lidar a Wollaston prism is installed, which divides the received backscattered radiation into two orthogonally polarized beams. These radiation beams are recorded by two photomultiplier tubes (PMTs) operating in the photon counting mode with time strobing of the signal, which provides the lidar height resolution from 37.5 to 150 m. To suppress active backscatter noise from the lidar's near-field zone (up to 3 km), electro-optical shutters (EOS) [19] are installed in front of the PMT allowing the characteristics to remain linear even during lidar operation in the daytime at the maximum energy of the sensing pulse.

Pulses of radiation with four different polarization states (three linear and one circular) are sent to the atmosphere one by one. For each of them the polarization state of the backscattered radiation described by the Stokes vector is determined. Thus, 16 intensity vertical profiles are measured in each sensing cycle, from which 16 BSPM elements are calculated. In addition, other important cloud characteristics are determined based on the analysis of lidar measurement data: optical-scattering ratio and optical thickness, and geometrical-altitudes of the lower and upper boundaries, and thickness [20]. As noted in the Introduction, the horizontal orientation of ice particles in HLC leads to anomalous backscattering of optical radiation when sensing into the zenith. Based on HAMPL sensing data, such clouds are identified if the following criteria are simultaneously met: scattering ratio $R > 10$, optical thickness $\tau < 1$, and BSPM element $m_{44} < -0.4$ [15,20].

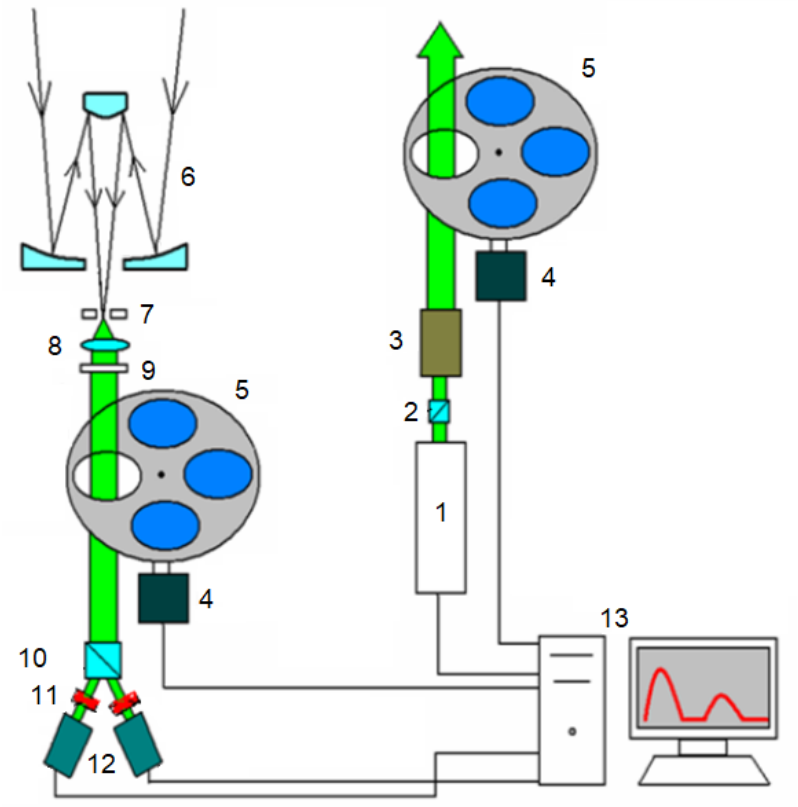

Figure 1. HAMPL block diagram: 1 – laser; 2 – Glan–Taylor prism; 3 – collimator; 4 – stepping motor; 5 – polarization transformation, 6 – Cassegrain telescope; 7 – field stop; 8 – lens; 9 – interference filter; 10 – Wollaston prism; 11 – PMT; 12 – EOS; 13 – computer-based data recording and displaying equipment [15,21].

Table 1. Main characteristics of the HAMPL developed at NR TSU [22,23].

Transmitting system			
Laser type		YAG:Nd3+; Lotis TII LS-2137U	
Wavelength, nm	**Energy, mJ**	**Pulse repetition rate, Hz**	10
1064	700	**Divergence of the beam, mrad**	0.8
532	400	**Divergence of the beam after the collimator, mrad**	0.28
355	160		
266	120	**Pulse duration**, ns	7
Receiving system			
Type of registering device	Two-channel photon counter Becker & Hickl GmbH PMS-400A	**Type of interference filter**	Thorlabs FL532-3
Count rate, MHz	800	**Central wavelength, nm**	532 ± 0.6
Minimum width of the strobed pulse, ns	1	**Bandwidth, nm**	3 ± 0.6
Electro-optical shutter			
Crystal material	DKDP	**Maximum frequency of trigger pulse, Hz**	100
Crystal dimensions, mm	15×15×30	**Duration of high voltage pulse, μs**	1÷1000
Operating wavelengths, nm	355, 532, 1064	**Delay of the high voltage pulse relative to the trigger pulse, μs**	1÷100

The HAMPL receiver of the backscattered laser radiation provides the required accuracy of the lidar signal registration from both near- and far-lying layers of the atmosphere. One way to match the dynamic range of the lidar signal and the lidar photodetector system is a range gating of the transmission function of the lidar optical system. Since in the HAMPL receiving system the backscattered radiation is separated into two orthogonally polarized components, the use of EOS based on the Pockels effect seems to be the most optimal. The use of this type of EOS (custom-made by Lotis TII) in the HAMPL allows to obtain an acceptable value of the gate response time in the range of 20-50 ns. The main characteristics of the lidar components are shown in Table 1.

The use of the polarization state transformation blocks of the sent and received beams makes it possible to obtain all 4 components of the Stokes vector of the backscattered radiation and, thus, to determine the total BSPM of the cloud layer. In this case, use of the Wollaston prism provides a possibility to obtain the Stokes vectors in two mutually orthogonal channels of the receiving system simultaneously, which significantly increases the reliability of the obtained data. Figure 2 shows the vertical lidar signal intensity profiles for each combination of the sensing radiation polarization state (described by the Stokes vector $\vec{S}$), and the instrument vector G of the lidar receiver system for both HAMPL receiver channels. The instrument vectors G are given only for the first receiving channel, as indicated by the upper index "A". For the second channel, they correspond to $G^{(A)}$, but have opposite signs for all components except the first. Note that the intensity of the lidar signal for altitudes below 3 km is significantly reduced, which is caused by the work of EOS suppressing active noise from the lower atmosphere.

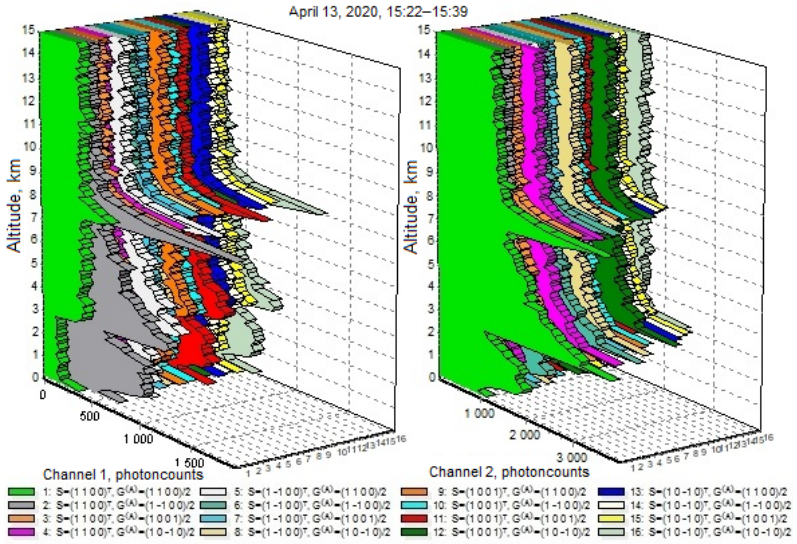

Figure 2. Example of vertical lidar signal intensity profiles for different combinations of polarization states of the sensing and received backscattered radiation for both channels of the HAMPL receiver system.

During experiments on obtaining BSPM, it should be taken into account a continuous change of the volumes of air from which scattered radiation comes during the time interval required to obtain all 16 elements of the matrix. A correct obtaining of BSPM requires "freezing" conditions, i.e., position and orientation of the particles remain unchanged during the measurement period. It is practically impossible to strictly comply with this condition in a remote sensing scheme [24], since a sequential change of the polarization state of the lidar radiation is required. Scattering properties of the aerosol ensemble change chaotically even in absence of macroscopic transfer, and therefore, an averaging of the BSPM elements over the fluctuation time is inevitable. Thus, the involved number of particles may vary from measurement to measurement. For this reason, early studies at HAMPL were based on the hypothesis that the microphysical characteristics of the particles, responsible for the polarization of the radiation, are conserved in the general ensemble, and there are only variations in their concentrations.

In 2016, the HAMPL implemented a mode of the "parallel" accumulation of the 16 lidar signals from HLC with the same accuracy at the same time interval. In this mode the minimal time for measuring the full BSPM becomes 2 seconds. Thus, the motion of the investigated air volumes in the field of view of the telescope affects equally all measurements for all combinations of polarizations of the transmitted and received radiation. Figure 3 shows an example of dynamics of the lidar signal vertical intensity profile.

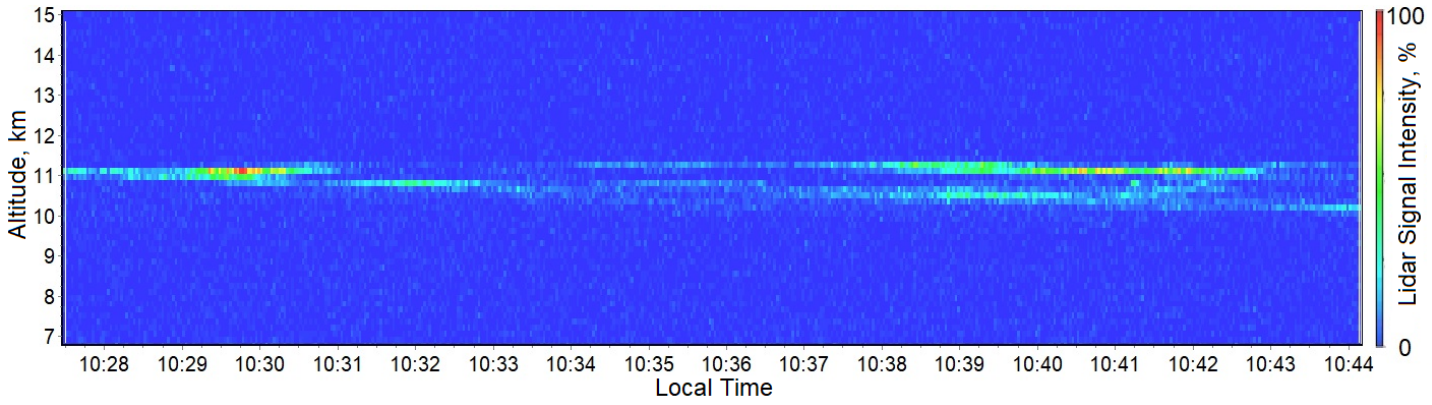

Figure 3. Example of timeline dynamics of lidar signal vertical profile (September 9, 2020).

In addition, the parallel signal recording makes it possible to conduct a long continuous session of HLC sensing, and then select the most promising time intervals for processing. This procedure allowed us to establish that the same lengthy cloud can contain both specular (containing horizontally oriented ice particles) and non-specular local areas, as well as to estimate their sizes [25,26].

2.2. Use of meteorological data for interpretation of lidar data

Study of the cloud properties requires a combined analysis with the meteorological data at the corresponding altitudes. The most reliable and extremely important source of information on the vertical profiles of meteorological data is the radiosonde observations. At present, the Russian radiosonde network includes 127 aerological stations on the territory of the Russian Federation and two more in Antarctica [27]. To estimate the meteorological conditions at the altitudes of the investigated HLC, until recently, we used the measurements of the aerological stations closest to Tomsk located in Kolpashevo (WMO 29231) and Novosibirsk (WMO 29634).

2.2.1. Radiosonde observations

Figure 4 shows a map of the aerological station locations within the 500 km radius from Tomsk; their distances from the HAMPL standing point are given in Table 2. Aerological data are freely available on the website of the University of Wyoming (USA), which provides access to measurement data performed all over the globe since 1973. [15,28].

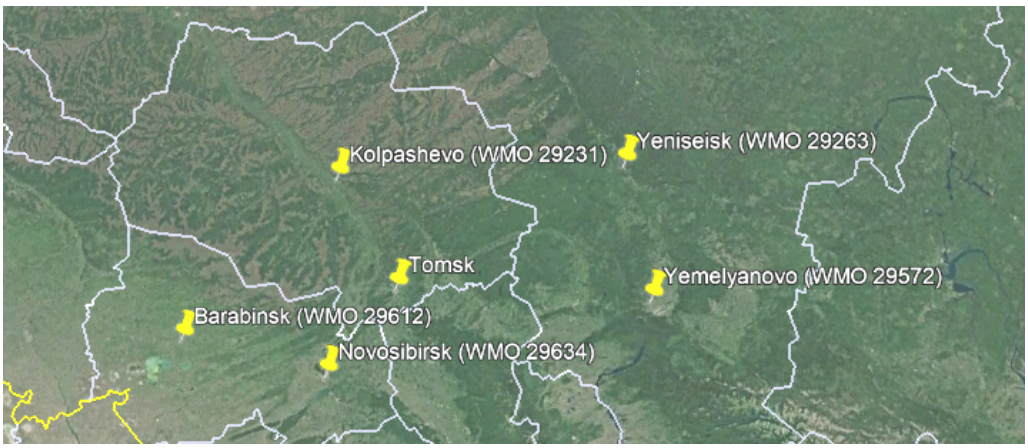

Figure 4. Location of aerological stations closest to Tomsk according to the data from the website [29].

Table 2. Aerological stations located within a radius of 500 km from Tomsk.

Station location	Station ID	Distance from the station to Tomsk, km
Novosibirsk	WMO 29634	210
Kolpashevo	WMO 29231	240
Barabinsk	WMO 29612	430
Yemelyanovo	WMO 29572	470
Yeniseisk	WMO 29263	480

In spite of remoteness of the aerological stations of Novosibirsk and Kolpashevo from each other, the meteorological conditions at the altitudes of HLC formation based on the data of both stations usually differ insignificantly [15,26]. To illustrate the small differences in the vertical profiles of meteorological values from data of these stations, Figure 5 shows examples of temperature vertical profiles and wind direction measured at these stations.

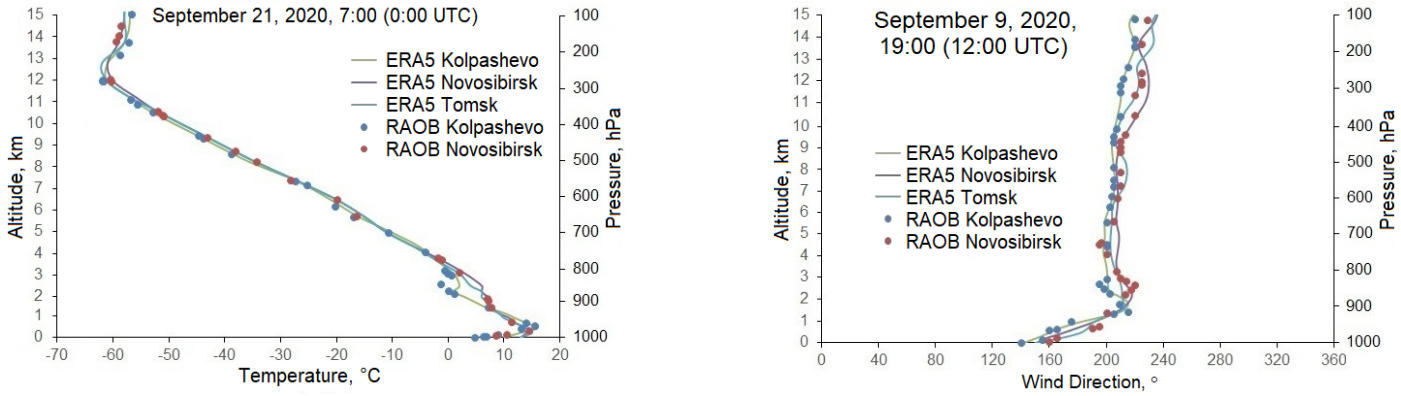

(a) **(b)**

Figure 5. Vertical profiles of temperature (**a**) and wind direction (**b**) from data of the radiosonde observations (RAOB) and reanalysis (ERA5) for the Kolpashevo, Novosibirsk and Tomsk coordinates [30].

The similarity of meteorological measurements of two mentioned aerological stations does not take place always. In addition, measurements at them are performed only twice a day - at 0:00 and 12:00 UTC (7:00 and 19:00 local time). Thus, a comparison of the cloud characteristics determined from the lidar data with the vertical profiles of the meteorological data often requires a choice: data from which station and for which time should be used. This choice becomes more important when estimating the drift parameters of the aerosol formations. Such an assessment is performed for the identification and study of contrails (e.g., [31]), as well as for the temporal correction of the results of complex lidar-pyranometer experiments [26].

2.2.2. Meteorological conditions of formation of preferred horizontal orientation of ice particles in HLC

During 2016-2020, about 1500 series of measurements (including measurements in cloudless conditions; one series of measurements usually takes 17 minutes) were performed at HAMPL in the regime of "parallel" lidar signal accumulation [32]. Figure 6 shows distributions of the measurements series by year and by season. Despite the predominance of the lidar measurement series in spring, the largest number of HLC by absolute value was detected in winter and about 20% less in autumn. At the same time, the largest number of specular areas of clouds was detected in autumn, while in spring, on the contrary, the number was the smallest one. In summer, both the number of detected HLC and the number of their specular areas were significantly smaller, but the second number exceeds the first one [32].

As noted in Section 2.1, the parallel accumulation of lidar signals makes it possible to conduct long continuous sessions of HLC sensing and then select the most promising time intervals for processing. The joint analysis of the duration lidar detecting of a specular local area of HLC and the altitude of its location with the wind speed at this altitude based on the radiosonde observations data provides a possibility to estimate the size of such areas. HLC were detected during 231 series of measurements (see Figure 6); 81 specular areas of such clouds were identified and their sizes were estimated. The distribution of HLC specular area size estimates is shown in Figure 7. Since the data from two aerological stations closest to the HAMPL location were used, the histogram shows data from both of them. The sizes of the HLC specular areas lie in the range from 4 to 30 km; the fraction of cases with the largest value is 2% of the total number.

Figure 8 shows the distributions of the altitudes of the specular HLC formation according to lidar measurements, as well as the values of relative humidity, air temperature, and dew point at these altitudes. The most frequent specular HLC were observed at values

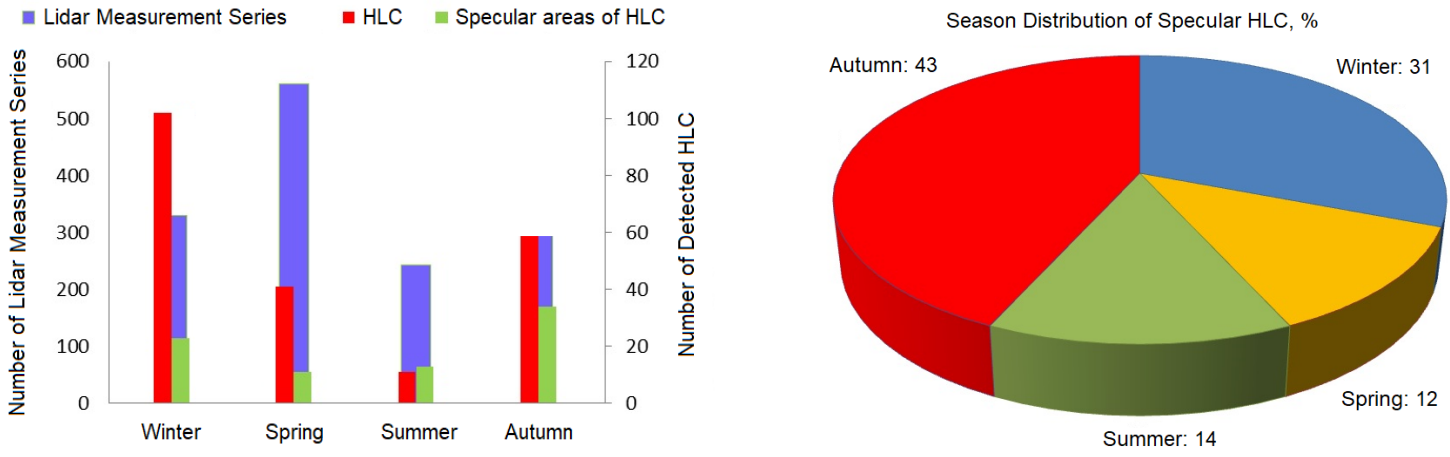

Figure 6. Distribution of the number of measurement series with parallel accumulation of photoelectron pulses at the HAMPL (**a**) and season distribution of specular HLC detected with the HAMPL in 2016–2022 (**b**) [32].

of air temperature and dew point of −60...−50°C and −70...−60°C, respectively, as well as at 30–40% relative air humidity [32].

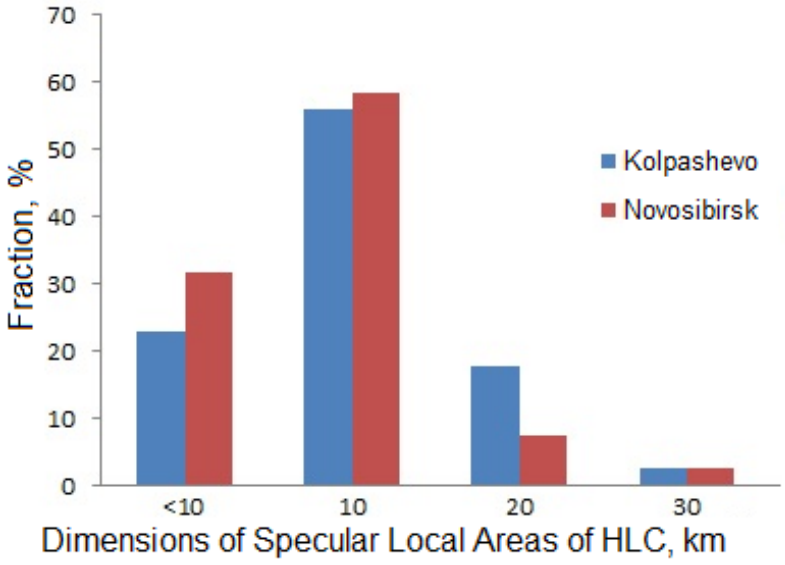

Figure 7. Distribution of HLC specular area sizes (2016-2020) [33].

The most frequent specular HLC were recorded at the altitudes of 10–11 and 6–7 km. Most of the regular air traffic routes within a radius of 100 km from Tomsk are located at these altitudes [34]. Before COVID-19 pandemic about 200 airplanes per day flew here on average. Some contrail studies performed at HAMPL since 2016 are described in [31,35]. It is premature to estimate the relationship between the recurrence of specular HLC and air traffic at their altitudes, because the array of recorded aircraft trajectories (these data have been continuously recorded since August 2019) is much smaller than the lidar data time span. Also the density of air traffic within a radius of 100 km from Tomsk from March to December 2020 is about 1.5–2 times lower than before the pandemic [32].

2.2.3. ERA5 Reanalysis

Previously, in search for a source of a meteorological data alternative to the aerological measurements, the applicability of reanalysis was tested to interpret data from the lidar

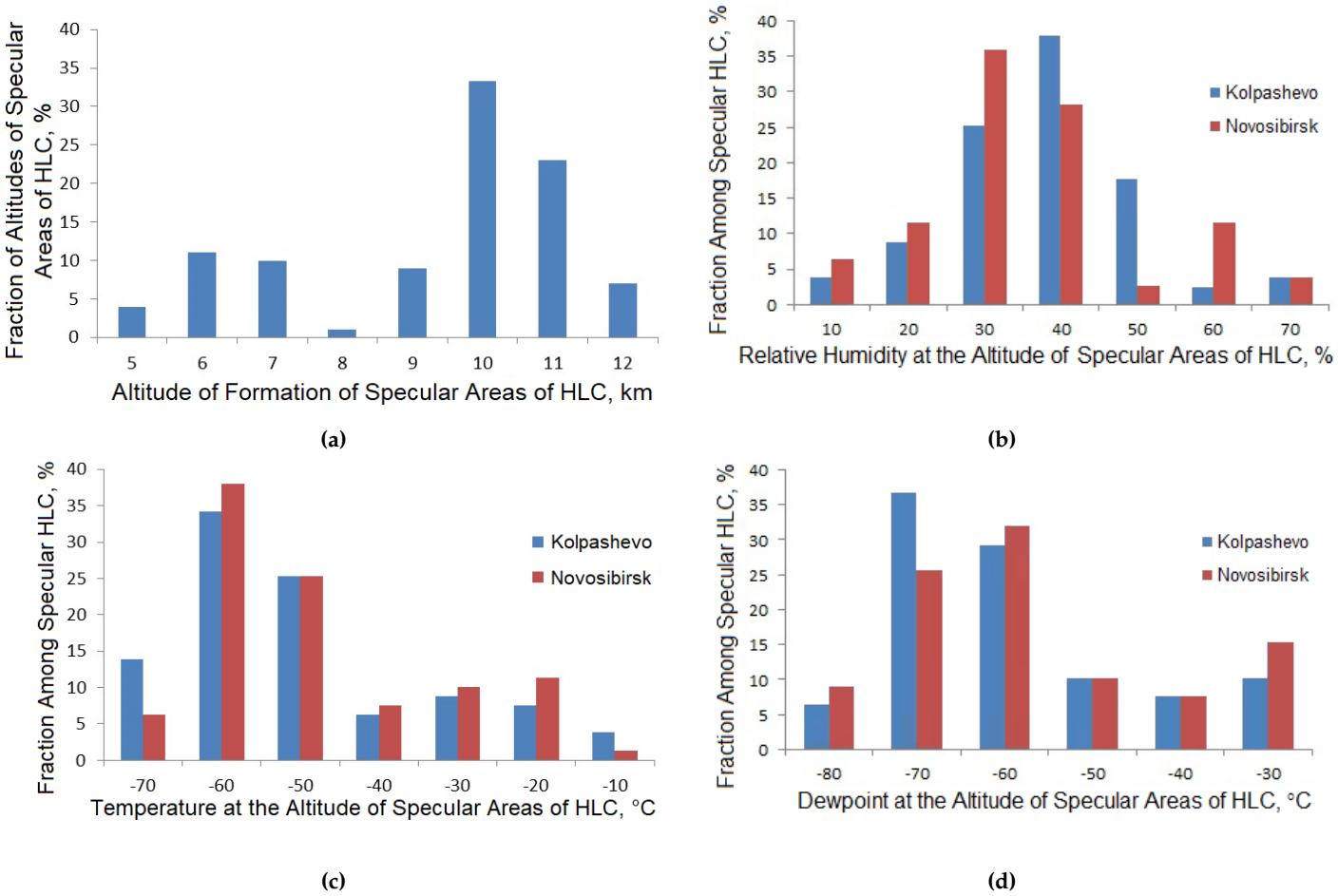

Figure 8. Distribution of of altitudes of HLC with horizontally oriented ice particles detected with HAMPL (**a**) and corresponding values of relative humidity (**b**), air temperature (**c**), and dew point (**d**) at their altitudes based on the data from aerological stations (2016-2020) [28,32].

experiments. Such data sets combine the results of measurements from many meteorological instruments around the globe and use different systems for processing the information. The ERA (short for ECMWF ReAnalysis), specifically the ERA-Interim version [36], was used for the reanalysis verification: the data for Kolpashevo, Novosibirsk, and Tomsk were compared with the corresponding RAOB data. It was shown [31], that the temperature, the wind direction, and wind speed at the altitudes of HLC formation agree well with each other for the indicated coordinate points and for both sources of vertical meteorological profiles used.

ERA-Interim reanalysis data are available for the period from January 1, 1979 to August 31, 2019. They are developed in the fifth generation ERA5 reanalysis, which provides high spatial resolution ($0.25^\circ \times 0.25^\circ$), more frequent time step (1 hour). It includes integration of continuous series of meteorological data for the period of more than 40 years (from 1979 to the present). As input data for the ERA5 reanalysis, the results of the measurements from all over the globe are used: satellite radiometers, ground, ship, and airborne weather stations, moored buoys, radiosondes, and ground-based radars [37]. In addition, similar ERA5 series were calculated for the period 1950-1978, but, due to the limited accumulated data for this period, the accuracy of this part of the array is worse than that of the main set. Time series of the air temperature and its derivatives in the reanalyses of the ERA family are homogeneous for the territory of Siberia, and, therefore, can be used to identify spatial heterogeneity due to local factors [38].

3. Results

To assess the applicability of the ERA5 reanalysis for the interpretation of HAMPL measurement data, the RAOB and ERA5 data were compared. The values of the temperature, the relative and specific humidity, as well as the wind direction and speed on standard isobaric surfaces from 1000 to 50 hPa were analysed. This pressure range approximately corresponds to the altitudes from 0 to 20 km and includes the operating range of the HAMPL (0–15 km). An array of the meteorological information combines data for all days from January 1, 2016 to December 31, 2020, two time moments (corresponding to the time of measurements at the aerological stations – 00:00 and 12:00 UTC) in each of five coordinate points (points of aerological stations location shown in Figure 4 and Table 2). Statistical analysis of the obtained data was carried out: similarly to [30,39], vertical profiles of the standard deviations of ERA5 meteorological values from RAOB ones, as well as the average difference and the correlation coefficient of these values were obtained.

In order to perform the analysis, a local database was created. It has an irregular step of the atmospheric pressure in the RAOB data and occasional omissions in them. To mitigate the influence of these features, a preliminary selection of data was made: vertical profiles from ERA5 and RAOB data arrays for the same place and time were matched. Then, for each atmospheric pressure in the ERA5 data, the nearest pressure from the RAOB data array was searched for. If the pressure difference exceeded 7.5 hPa, this pair of values was excluded from further analysis. In addition, this pressure level in the RAOB data was excluded from comparison with ERA5 data for other levels. Thus, as a result of the selection we have pairs of values of the meteorological quantities based on the ERA5 and RAOB datasets, which can be compared with each other.

The standard deviation of the values was calculated by the formula:

$$RMSE = \sqrt{\frac{1}{N_s}\sum_{i=1}^{N_s}\left(X_i^{RAOB} - X_i^{ERA5}\right)^2}. \quad (1)$$

The mean difference of the values showing the sign of deviations was calculated as follows:

$$Bias = \frac{1}{N_s}\sum_{i=1}^{N_s}\left(X_i^{RAOB} - X_i^{ERA5}\right). \quad (2)$$

The correlation coefficient was determined by the formula:

$$Corr(ERA5, RAOB) = \frac{\sum_{i=1}^{N_s}\left(X_i^{ERA5} - \overline{X_i^{ERA5}}\right)\sum_{i=1}^{N_s}\left(X_i^{RAOB} - \overline{X_i^{RAOB}}\right)}{\sqrt{\sum_{i=1}^{N_s}\left(X_i^{ERA5} - \overline{X_i^{ERA5}}\right)^2\sum_{i=1}^{N_s}\left(X_i^{RAOB} - \overline{X_i^{RAOB}}\right)^2}} \quad (3)$$

Figures 9–13 show the vertical profiles of RMSE, Bias, and Corr, as well as the corresponding distributions of deviations of the absolute and relative humidity, the air temperature, the wind direction, and the wind speed based on ERA5 [40] relative to RAOB [28] data for 2016–2020 for the aerological stations specified in Table 2.

The analysis of the obtained vertical profiles of statistical characteristics describing accuracy of the recovery of the meteorological values by the ERA5 reanalysis is presented below.

4. Discussion

Using the standard deviation (RMSE) value as an accuracy measure for recoverying the meteorological quantity by ERA5 reanalysis, we note that the specific air humidity is recovered (Figure 9a) with an accuracy of 0.5–1 g/kg at isobaric levels of 1000–800 hPa, which corresponds to an altitude range of 0–2 km from sea level in the standard atmosphere.

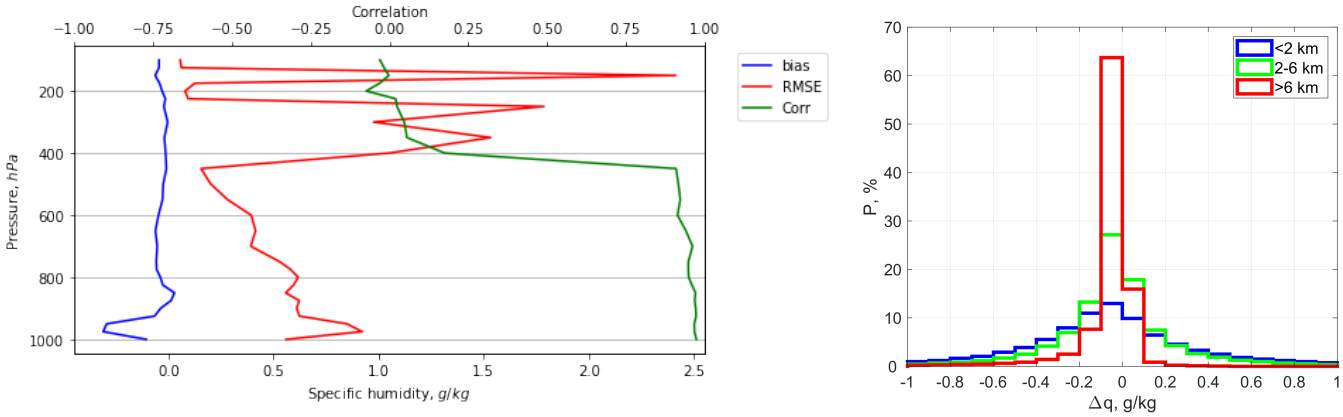

(a) **(b)**

Figure 9. Vertical profiles of RMSE, Bias, and Corr for the values of specific humidity based on ERA5 [40] relative to RAOB [28] data for 2016–2020 years (**a**) and the corresponding distribution of deviations Δq (**b**) for the coordinates of the mentioned aerological stations.

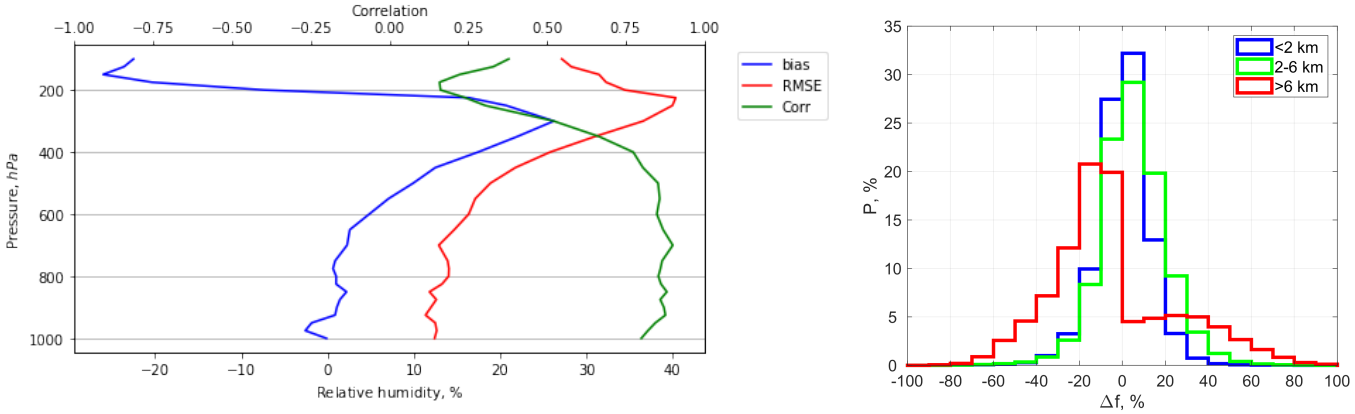

(a) **(b)**

Figure 10. Vertical profiles of RMSE, Bias, and Corr for the values of relative humidity based on ERA5 [40] relative to RAOB [28] data for 2016–2020 years (**a**) and the corresponding distribution of deviations Δf (**b**) for the coordinates of the mentioned aerological stations.

At the higher levels, up to the level of 450 hPa (about 6 km in the standard atmosphere), the accuracy improves: the RMSE takes values in the range of 0.3–0.7 g/kg. However, then the vertical profile behaviour of the RMSE of specific humidity changes sharply: it takes values from 0.2 to 2.4 g/kg. At the same time, the correlation coefficient *Corr* insignificantly fluctuating around unity below the heights of HLC formation (at isobaric levels above 450 hPa) also demonstrates a sharp deterioration of the relationship between the recovered and measured values of specific humidity above this level reaching zero or even negative values there. The magnitude of the average difference *Bias* at the levels of 1000–800 hPa varies from −0.3 to 0 showing slight variations from −0.1 to 0 above up to the very top of the indicated pressure range. According to Figure 9b, there is most often an underestimation of the specific humidity values from ERA5 compared to RAOB. The highest repeatability is in the deviations of specific humidity values (Δq) obtained from ERA5 reanalysis relative to similar values from RAOB data in the range −0.2...0.1 g/kg at all levels (0–2 km, 2–6 km, and over 6 km). With a probability of more than 5% there are Δq values in the ranges −0.4...0.2 g/kg, −0.3...0.2 g/kg, and −0.2...0.1 g/kg for the lower, middle, and upper levels, respectively. Thus, for the specific air humidity, the range of isobaric levels of the most reliable recovery at the considered coordinate points under consideration and for the considered time period is 800–450 hPa (2–6 km in the standard atmosphere). This range

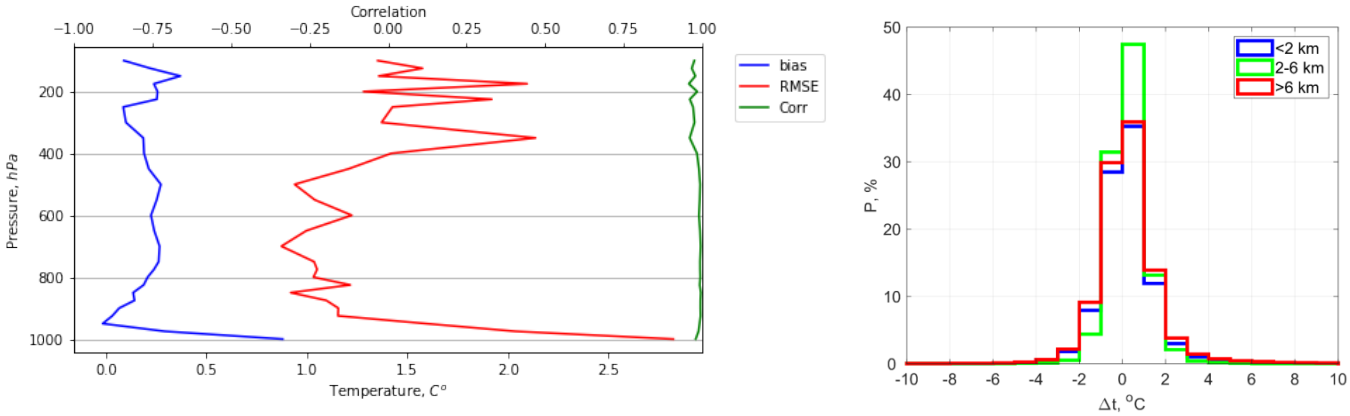

(a) **(b)**

Figure 11. Vertical profiles of RMSE, Bias, and Corr for the values of temperature based on ERA5 [40] relative to RAOB [28] data for 2016–2020 years (**a**) and the corresponding distribution of deviations Δt (**b**) for the coordinates of the mentioned aerological stations.

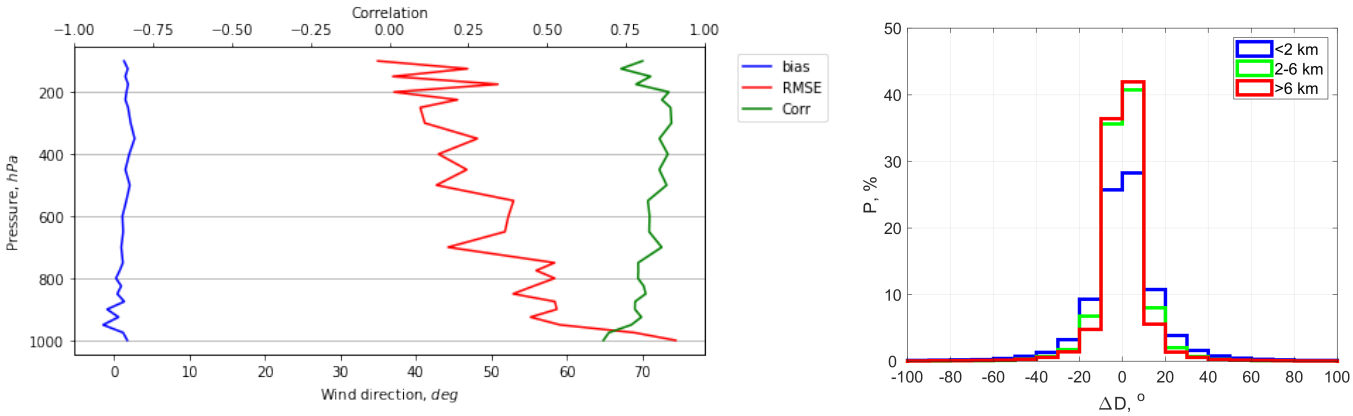

(a) **(b)**

Figure 12. Vertical profiles of RMSE, Bias, and Corr for the values of wind direction based on ERA5 [40] relative to RAOB [28] data for 2016–2020 years (**a**) and the corresponding distribution of deviations ΔD (**b**) for the coordinates of the mentioned aerological stations.

includes only a small part of the height range of HLC formation and therefore is not useful for interpreting the data of lidar studies of such clouds

Relative humidity is characterised (Figure 10a) by smoother vertical profiles of the considered statistical characteristics. Nevertheless, it is impossible to call them applicable for interpretation of HLC lidar data. The lowest values of RMSE (11–15%), as well as Bias (−8...2%) are achieved at levels 1000–800 hPa, corresponding to lower altitudes. As the isobaric level increases (up to about 200 hPa), the RMSE increases almost continuously, reaching completely unacceptable values around 40%. Bias behaves similarly reaching a maximum value of 25% at a lower level (300 hPa). The Corr value in the considered range of isobaric levels has the highest value of about 0.87 at about 700 hPa. Wherein, for isobaric levels corresponding to the altitude range of HLC formation heights (450–200 hPa), this value varies from 0.75 at the bottom of the range to 0.15 at its upper boundary. According to Figure 10b, the lower and middle levels (0–2 km and 2–6 km) are usually characterized by overestimation of the relative humidity from ERA5 compared to RAOB, and the upper level (more than 6 km) is characterized by underestimation. The greatest repeatability is in the deviations of relative humidity values (Δf) obtained from ERA5 reanalysis relative to similar values from RAOB data in the ranges of $0 \div 10\%$ (for the lower and middle levels) and $-20...-10\%$ (for the upper level). With a probability of more than 5% Δf values in the

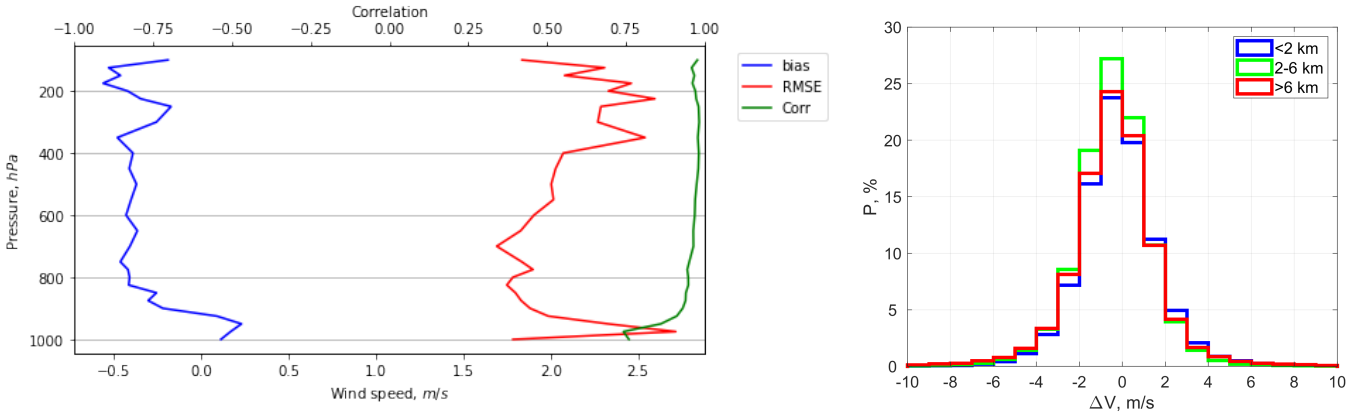

(a) **(b)**

Figure 13. Vertical profiles of RMSE, Bias, and Corr for the values of wind speed based on ERA5 [40] relative to RAOB [28] data for 2016–2020 years (**a**) and the corresponding distribution of deviations ΔV (**b**) for the coordinates of the mentioned aerological stations.

ranges of −20...20%, −20...30% and −40...0% are observed for the lower, middle, and upper levels, respectively. Thus, the use of vertical profiles of relative humidity base on ERA5 data for interpretation of HLC laser sensing data seems to be incorrect.

Describing the accuracy of the temperature recovery (Figure 11a), we note the small RMSE values (0.8–2.8°C) and extremely small fluctuations of the Corr values around unity in the entire considered range of isobaric levels, which is known to characterize the very high accuracy of the ERA5 data. Nevertheless, here we consider the fluctuations of the vertical profiles of the examined statistical characteristics in more detail. The vertical RMSE profile experiences fluctuations with the greatest amplitude in the range of 0.9–2.8°C at levels of 1000–800 hPa. At higher altitudes, up to an isobaric level of 450 hPa, the range of the temperature RMSE values is 0.9–1.4°C, from 450 to 200 hPa – 1.4–2.1°C. The Bias value shows fluctuations with even smaller amplitude: 0–0.9°C for isobaric levels of 1000–800 hPa, 0.2–0.3°C for levels of 800–450 hPa, and 0.1–0.5°C below 450 hPa. According to Figure 11b, the overestimation of air temperature values based on ERA5 data relative to RAOB is most often observed. The highest repeatability is observed for deviations of air temperature values (Δt) obtained from ERA5 reanalysis relative to similar values from RAOB data in the range of $0 \div 1°C$ at all levels (0–2 km, 2–6 km, and more than 6 km). There is more than 5% probability of Δt values in the ranges −2...2°C, −1...2°C and −2...2°C for lower, middle, and upper levels respectively. Obtained results demonstrate a very high accuracy of temperature recovering by ERA5 reanalysis in the entire considered range of altitudes, and therefore we evaluate these data as applicable for the analysis of HLC laser sensing results. We emphasize that temperature is one of the most important meteorological parameters when analyzing the conditions for forming the preferred orientation of ice particles in clouds. In addition, shapes of such particles are also often associated specifically with temperature (e.g. [41]).

Analyzing about the wind direction (Figure 12a), we note the unacceptably high RMSE values in the whole considered range of altitudes. Thus, at isobaric levels of 1000–800 hPa, this value takes values of 52–75°. Higher, up to 450 hPa, the RMSE fluctuations slightly decrease: the range of its values here is 42–57°, and at higher levels – 35–50°. The vertical profile of the wind direction Bias is noteworthy: at isobaric levels of 1000–800 hPa, this value varies from −1 to 1°, and – from 0 to 3° at higher levels, which could be considered insignificant if RMSE did not behave as described above. The Corr value at isobaric levels of 1000–800 hPa varies in the range of 0.63–0.77. At higher levels, up to a pressure of 450 hPa, as for the RMSE the situation improves slightly: Corr ranges from 0.75 to 0.85. At higher altitudes, the variability of Corr values is slightly greater: 0.74–0.86. According to Figure 12b, an overestimation of the wind direction values based on the ERA5 data

relative to RAOB is usually observed. The greatest recurrence is in the deviations of wind direction values (ΔD) obtained from the ERA5 reanalysis relative to similar values from RAOB data in the range of $0 \div 10^{\circ}$ at all levels (0–2 km, 2–6 km, and more than 6 km). With a probability of more than 5%, ΔD values in the range of $-30...30^{\circ}$ for the lower and middle levels, and $-20...20^{\circ}$ for the upper level are observed. To summarize the analysis of the wind direction based on the ERA5 data, we conclude that in the range of altitudes of HLC formation, the differences of the recovered values often differ significantly from those measured by radiosondes, and therefore their applicability to lidar data analysis is limited, although not impossible. A recommendation is to compare these ERA5 data with the results of the radiosonde observations closest in time made at the stations closest to the HLC study location.

The wind speed (Figure 13a) is characterized by an even more pronounced difference in the behavior of the vertical profiles of all considered statistical quantities in three examined pressure intervals. In particular, the RMSE varies in the range of 1.8–2.8 m/s at isobaric levels of 1000–800 hPa. A similar situation is also observed at levels of 450–200 hPa: the RMSE takes values of 2–2.5 m/s. At the same time, for pressures of 800–450 hPa, the vertical profile of RMSE shifts noticeably towards lower values indicating a higher recovery accuracy: 1.7–2 m/s. It is remarkable that the correlation coefficient (Corr) drops to an unacceptable value of 0.75 only at isobaric levels of 1000–800 hPa. At higher layers, up to 450 hPa, this value increases all the time, reaching a value of 0.95. From 450 to 200 hPa Corr is still close to 0.95 and only above 200 hPa this value slightly decreases. Analysis of the Bias vertical profile behavior leads to a similar observation: at isobaric levels between 1000 and 800 hPa the largest variations occur (from -0.5 to 0.2 m/s), and the area of highest accuracy (Bias values from -0.5 to -0.4) is in the level range of 800-450 hPa. In general, the whole range of variation of Bias from -0.5 to 0.2 m/s does not cause any doubt about the accuracy of wind speed recovering. According to Figure 13b, there is usually a slight underestimation of the wind speed values based on the ERA5 data relative to RAOB. The highest repeatability is in the deviations of wind speed values (ΔV) obtained from ERA5 reanalysis relative to similar values from RAOB data in the range $-1...0$ m/s at lower, middle, and upper levels (0–2 km, 2–6 km, and more than 6 km). ΔV values in the range of $-3...2$ m/s are observed at all levels with a probability of more than 5%. Thus, the accuracy of wind speed recovery by ERA5 reanalysis is acceptable for the height range of HLC formation.

5. Conclusion

The presented results show a promising application of the vertical profiles of the temperature and the wind speed based on the ERA5 reanalysis data for the HLC studies. It is possible to use these data for the Tomsk coordinates for interpretation of the experimental data performed on the HAMPL developed at NR TSU. In addition, the use of the ERA5 data will improve the temporal resolution of the meteorological part of the lidar-meteorological dataset from 12 h (RAOB) to 1 h (ERA5). Wind direction can also be used for such studies, but as commented above, an additional comparison with the radiosonde observations may be necessary. Alas, vertical profiles of the specific and relative humidity show significant discrepancies from those measured by radiosondes, and therefore we cannot conclude about correctness of its usage.

Although the described results are obtained for the region presented in Figure 4, they can be extended to the whole of Western Siberia. However, we admit that a similar verification of the ERA5 data for other regions may show different results. In addition, we should keep in mind the limited time interval of the considered data sample: only meteorological data for 2016–2020 period were analyzed. We suppose that expanding the time range may also affect such analysis. The data sample used in this article, which combines measurements and calculations for each day during 5 years and for 5 cities, is certainly representative. Therefore, possible deviations of the results obtained from extended data samples are not expected to be significant. This statement is confirmed by

the consistency of the results of the current analysis with those obtained earlier for a smaller data set [34].

Author Contributions: I. Bryukhanov (I.B.), O. Kuchinskaya (O.K.), and I. Samokhvalov (I.S.) developed the idea for this paper. I. Bryukhanov (I.B.), E. Ni (E.Ni), N. Kirillov (N.K.), I. Zhivotenyuk (I.Zh.), A. Stykon (A.S.), and I. Samokhvalov (I.S.) developed the experimental methods, constructed the HAMPL of TSU and performed lidar measurements. I. Bryukhanov (I.B.), M. Penzin (M.P.), E. Ni (E.N.), K. Pustovalov (K.P.), and A. Doroshkevich (A.D.) developed software for data processing, visualization, and validation. I. Bryukhanov (I.B.), M. Penzin (M.P.), O. Kuchinskaya (O.K.), K. Pustovalov (K.P.), and V. Bryukhanova (V.B.) and I. Samokhvalov (I.S.) analyzed the measurement and computation data. I. Bryukhanov (I.B.), M. Penzin (M.P.), O. Kuchinskaya (O.K.), N. Kirillov (N.K.), K. Pustovalov (N.K.), Yu Bordulev (Iu.B.), V. Kostyukhin (V.K.), V. Brukhanova (V.B.), and I. Samokhvalov (I.S.) discussed their results and wrote and edited the paper.

Funding: The work was performed with the financial support of the Russian Science Foundation, Grant No. 21-72-10089.

Conflicts of Interest: The authors declare no conflict of interest.

Abbreviations

The following abbreviations are used in this manuscript:

BSPM	Backscattering Phase Matrix
EOS	Electro-Optical Shutters
ERA	ECMWF ReAnalysis
HAMPL	High-Altitude Matrix Polarization Lidar
HLC	High-Level Clouds
NR TSU	National Research Tomsk State University
PMT	Photomultiplier Tube
RAOB	Radiosonde Observations

References

1. Dmitrieva-Arrago, L.R.; Trubina, M.A.; Tolstyh, M.A. Role of Phase Composition of Clouds in Forming High and Low Frequency Radiaion. *Proceedings of the Hydrometeorological Research Center of the Russian Federation* **2017**, pp. 19–34. (in Russian).
2. Liou, K.N. Influence of Cirrus Clouds on Weather and Climate Processes: A Global Perspective. *Monthly Weather Review* **1986**, *114*, 1167 – 1199. doi:10.1175/1520-0493(1986)114<1167:IOCCOW>2.0.CO;2.
3. Wylie, D.P.; Menzel, W.P.; Woolf, H.M.; Strabala, K.I. Four Years of Global Cirrus Cloud Statistics Using HIRS. *Journal of Climate* **1994**, *7*, 1972 – 1986. doi:10.1175/1520-0442(1994)007<1972:FYOGCC>2.0.CO;2.
4. Reichardt, J.; Reichardt, S.; Lin, R.F.; Hess, M.; McGee, T.J.; Starr, D.O. Optical-Microphysical Cirrus Model. *Journal of Geophysical Research: Atmospheres* **2008**, *113*, D22201:1–D22201:17. doi:10.1029/2008JD010071.
5. Stocker, T.F.; Qin, D.; Plattner, G.K.; Tignor, M.; Allen, S.K.; Boschung, J.; Nauels, A.; Xia, Y.; Bex, V.; Midgley, P.M., Eds. *Climate Change 2013 – The Physical Science Basis: Working Group I Contribution to the Fifth Assessment Report of the Intergovernmental Panel on Climate Change*; Cambridge University Press: Cambridge, UK, 2014. doi:10.1017/CBO9781107415324.
6. Shanks, J.G.; Lynch, D.K. Specular Scattering in Cirrus Clouds. In Proceedings of the Passive Infrared Remote Sensing of Clouds and the Atmosphere III; Lynch, D.K.; Shettle, E.P., Eds. International Society for Optics and Photonics, SPIE, 1995, Vol. 2578, pp. 227 – 238. doi:10.1117/12.228943.
7. Heymsfield, A.J.; Krämer, M.; Luebke, A.; Brown, P.; Cziczo, D.J.; Franklin, C.; Lawson, P.; Lohmann, U.; McFarquhar, G.; Ulanowski, Z.; et al. Cirrus Clouds. *Meteorological Monographs* **2017**, *58*, 2.1 – 2.26. doi:10.1175/AMSMONOGRAPHS-D-16-0010.1.
8. Mitchell, D.L.; Finnegan, W. Modification of Cirrus Clouds to Reduce Global Warming. *Environmental Research Letters* **2009**, *4*, 045102:1–045102:8. doi:10.1088/1748-9326/4/4/045102.
9. Storelvmo, T.; Kristjansson, J.E.; Muri, H.; Pfeffer, M.; Barahona, D.; Nenes, A. Cirrus Cloud Seeding has Potential to Cool Climate. *Geophysical Research Letters* **2013**, *40*, 178–182. doi:10.1029/2012GL054201.
10. Vorobyova, V.V.; Volodin, E.M. Numerical Simulation of Influence on Climate with the Help of Change of Properties of High-Level Clouds in Base of IVM RAS Model. *Proceedings of the Hydrometeorological Research Center of the Russian Federation* **2017**, pp. 5–18. (in Russian).
11. Minnis, P.; Ayers, J.K.; Palikonda, R.; Phan, D. Contrails, Cirrus Trends, and Climate. *Journal of Climate* **2004**, *17*, 1671–1685. doi:10.1175/1520-0442(2004)017<1671:CCTAC>2.0.CO;2.
12. International Cloud Atlas. https://cloudatlas.wmo.int/en/homomutatus.html, accessed on February 03, 2022.

13. Kärcher, B. Formation and Radiative Forcing of Contrail Cirrus. *Nat Commun* **2018**, *9*, 1824:1–1824:17. doi:10.1038/s41467-018-04068-0.
14. Gierens, K.; Vázquez-Navarro, M. Statistical Analysis of Contrail Lifetimes from a Satellite Perspective. *Meteorologische Zeitschrift* **2018**, *27*, 183–193. doi:10.1127/metz/2018/0888.
15. Samohvalov, I.V.; Kaul, B.V.; Nasonov, S.V.; Zhivotenyuk, I.V.; Bryukhanov, I.D. Backscattering Light Matrix of Reflecting High-Level Clouds Consisting of Crystal Mostly Horizontally-Oriented Particles. *Atmospheric and Oceanic Optics* **2012**, *25*, 403–411. (in Russian).
16. Guasta, M.D.; Vallar, E.; Riviere, O.; Castagnoli, F.; Venturi, V.; Morandi, M. Use of Polarimetric Lidar for the Study of Oriented Ice Plates in Clouds. *Applied Optics* **2006**, *45*, 4878–4887. doi:10.1364/AO.45.004878.
17. Hayman, M.; Spuler, S.; Morley, B.; VanAndel, J. Polarization Lidar Operation for Measuring Backscatter Phase Matrices of Oriented Scatterers. *Optics Express* **2012**, *20*, 29553–29567. doi:10.1364/OE.20.029553.
18. Volkov, S.N.; Samokhvalov, I.V.; Cheong, H.D.; Kim, D. Investigation of East Asian Clouds with Polarization Light Detection and Ranging. *Applied Optics* **2015**, *54*, 3095–3105. doi:10.1364/AO.54.003095.
19. Kirillov, N.S.; Samokhvalov, I.V. Application of an Electro-Optical Shutter for Strobing of Lidar Signals. In Proceedings of the 20th International Symposium on Atmospheric and Ocean Optics: Atmospheric Physics; Romanovskii, O.A., Ed. International Society for Optics and Photonics, SPIE, 2014, Vol. 9292, pp. 92922D:1–92922D:5. doi:10.1117/12.2074605.
20. Samokhvalov, I.V.; Bryukhanov, I.D.; Nasonov, S.V.; Zhivotenyuk, I.V.; Stykon, A.P. Investigation of the Optical Characteristics of Cirrus Clouds with Anomalous Backscattering. *Russian Physics Journal* **2013**, *55*, 925–929. doi:10.1007/s11182-013-9902-1.
21. Nasonov, S.V. Optical Characteristics of High-Level Clouds and Its Connections with Meteorological Atmospheric Parameters. PhD thesis, Tomsk State University, Tomsk, 2015. (in Russian).
22. Becker & Hickl. https://www.becker-hickl.com/products/pms-400a, accessed on July 25, 2021.
23. Lotis TII. https://www.lotis-tii.com, accessed on January 23, 2022.
24. Kaul, B.V.; Kuznetsov, A.L.; Polovtseva, E.R.; Samohvalov, I.V. Investigation of Crystalline Clouds Based on Laser Radar Measurements of Backscattering Phase Matrices. *Atmospheric and Oceanic Optics* **1993**, *6*, 257–260.
25. Samokhvalov, I.V.; Bryukhanov, I.D.; Ni, E.V. Temporal Variability of the Specularity of High-Level Clouds According to the Data on Laser Polarization Sensing. In Proceedings of the 26th International Symposium on Atmospheric and Ocean Optics, Atmospheric Physics; Matvienko, G.G.; Romanovskii, O.A., Eds. International Society for Optics and Photonics, SPIE, 2020, Vol. 11560, pp. 115604C:1–115604C:5. doi:10.1117/12.2575529.
26. Bryukhanov, I.D.; Zuev, S.V.; Samokhvalov, I.V. Effect of Specular High-Level Clouds on Scattered Solar Radiation Fluxes at the Zenith. *Atmospheric and Oceanic Optics* **2021**, *34*, 327–334. doi:10.1134/S1024856021040059.
27. Chervyakov, M.Y. *Zondirovanie Atmosfery: Uchebno-Metodicheskoe Posobie Dlya Studentov, Obuchayuschihsya po Napravleniyu 05.03.05 Prikladnaya Gidrometeorologiya*; Nauka: Saratov, Russia, 2019. (in Russian).
28. University of Wyoming. http://weather.uwyo.edu, accessed on January 23, 2022.
29. Central Aerological Observatory. http://cao-ntcr.mipt.ru/monitor/locator.htm, accessed on January 23, 2022.
30. Loktyushin, O.Y.; Bryukhanov, I.D.; Nie, E.V.; Pustovalov, K.N.; Samokhvalov, I.V. Comparison of Aerology Data and ERA5 to Interpret Lidar Data. In Proceedings of the Modern Radioscience Problem: IX International Scientific and Practical Conference (Tomsk). TSU: Tomsk, Russia, 2021, pp. 180–184. (in Russian.
31. Samokhvalov, I.V.; Bryukhanov, I.D.; Park, S.; Zhivotenyuk, I.V.; Ni, E.V.; Stykon, A.P. Optical Characteristics of Contrails According to Polarization Lidar Sensing Data. In Proceedings of the 24th International Symposium on Atmospheric and Ocean Optics: Atmospheric Physics; Matvienko, G.G.; Romanovskii, O.A., Eds. International Society for Optics and Photonics, SPIE, 2018, Vol. 10833, pp. 108335J:1–108335J:6. doi:10.1117/12.2504517.
32. Samokhvalov, I.V.; Bryukhanov, I.D.; Ni, E.V.; Zhivotenyuk, I.V.; Doroshkevich, A.A.; Stykon, A.P. Analysis of Occurrence Frequency and Forming Condition of Reflective High Level Clouds Using Polarised Laser Sensing Data. *Trudy Voenno-Kosmicheskoy Akademii Imeni A. F. Mozhaiskogo* **2021**, *680*, 342–345. (in Russian).
33. Bryukhanov, I.D.; Nie, E.V.; Zivotenyuk, I.V.; Doroshkevich, A.A.; Stykon, A.P.; Kirillov, N.S.; Samokhvalov, I.V. Size Estimation of Reflection Area of High Level Clouds Using Polarised Laser Sensing Data. In Proceedings of the Modern Radioscience Problem: IX International Scientific and Practical Conference (Tomsk). TSU: Tomsk, Russia, 2021, pp. 189–192. (in Russian.
34. Flightradar24: Live air traffic. https://www.flightradar24.com, accessed on January 23, 2022.
35. Samokhvalov, I.V.; Bryukhanov, I.D.; Shishko, V.A.; Kustova, N.V.; Nie, E.V.; Konoshonkin, A.V.; Loktyushin, O.Y.; Timofeev, D.N. Estimation of Microphysical Characteristics of Contrails by Polarization Lidar Data: Theory and Experiment. *Atmospheric and Oceanic Optics* **2019**, *32*, 400–409. doi:10.1134/S1024856019040122.
36. The European Centre for Medium-Range Weather Forecasts. https://www.ecmwf.int, accessed on January 23, 2022.
37. ECMWF Confluence Wiki. ERA5: data documentation. https://confluence.ecmwf.int/display/CKB/ERA5%3A+data+documentation#ERA5:datadocumentation-Introduction, accessed on January 23, 2022.
38. Gordov, E.; Schukin, G.G.; Itkin, D.M.; Karavaev, D.M.; Chichikova, E.F. Analysis of Regional Climatic Processes of Syberia: Approach, Data and Some Results. *Vestnik Novosibirskogo Gosudarstvennogo Universiteta: Informatsionnye Tehnologii* **2011**, *9*, 56–66. (in Russian).

39. Schukin, G.G.; Itkin, D.M.; Karavaev, D.M.; Chichikova, E.F. Comparison of Satellite Data of Temperature-Humidity Atmospheric Sounding for North-West Russia. In Proceedings of the Materialy V Vserossiyskoy Nauchnoy Konferentsii (Murom, 26-28 June 2012), 2012, pp. 147–152. (in Russian).
40. Copernicus Climate Data Store. https://cds.climate.copernicus.eu, accessed on January 23, 2022.
41. Um, J.; McFarquhar, G.M.; Hong, Y.P.; Lee, S.S.; Jung, C.H.; Lawson, R.P.; Mo, Q. Dimensions and Aspect Ratios of Natural Ice Crystals. *Atmospheric Chemistry and Physics* **2015**, *15*, 3933–3956. doi:10.5194/acp-15-3933-2015.